Korean J. Chem. Eng., 40(3), 572-583 (2023)
DOI: 10.1007/s11814-022-1353-3

pISSN: 0256-1115
eISSN: 1975-7220

Breakdown of passivation for zinc-antimony alloy in alkaline batteries verification; galvanostatic, impedance spectra, and charge-discharge techniques

Mahmoud Elrouby*,,†, Hoda Abd El-Shafy Shilkamy*, and Abd El-Rahman El-Sayed*,†**

*Department of Chemistry, Faculty of Science, Sohag University, Sohag, 82524, Egypt
**King Salman International University, Faculty of Science, Ras Sudr, 46612, Sinai, Egypt
(*Received 13 August 2022 • Revised 8 November 2022 • Accepted 21 November 2022*)

Abstract−The passivation of pure zinc surface can be considered a problem of Zn utilization as an anode in alkaline batteries due to its small capacity. Therefore, to improve the discharge capacity of the Zn anode, minor Sb alloying with Zn was investigated. The impact of trace Sb alloyed with Zn on the passivity and the breakdown of the colloidal passive film on the surface was studied in concentrated KOH solution utilizing galvanostatic, electrochemical impedance spectroscopy (EIS), and galvanostatic charge-discharge measurements at the passivated area. The galvanostatic data show that the required time of passivation ($t_{pass.}$) is greater with increasing small Sb content in the alloy. The obtained results from electrochemical impedance spectroscopy (EIS) reveal that magnitudes of both resistivities of charge transfer (R_{ct}) and the impedance of Warburg (Z_w) decrease, while the magnitude of capacitance of double layer (C_{dl}) increases gradually with the increase in addition of small Sb to zinc metal. The evaluated data from the charging-discharging process show that the greatest value of potential height (ΔV) is for Zn-0.5%Sb alloy. Therefore, 0.5%Sb alloying with Zn can increase energy efficiency to a large extent than Zn and alloy II.

Keywords: Anodic Behavior, Passivity Breakdown, Antimony Alloyed with Zinc, EIS, Charge-discharge Process, Alkaline Batteries

INTRODUCTION

Zinc is used in electrical rechargeable Zn-air batteries due to its low cost, high safety, and high specific energy [1,2]. Bi-functional electrocatalysts for air-cathode electrodes have been focused on in many published papers [3-6]. On the other hand, the susceptibility of Zn as an anode electrode to physical deformation, dendrite formation, and corrosion processes has been studied [7-9]. Also, the use of Zn as an anode electrode in the battery has exhibited much influence on the behavior of the battery as a cathode electrode catalyst [10,11]. Zn electrode has a reversibility process, low equilibrium potential, and compatibility with an aqueous electrolyte. Accordingly, Zn has been used as an anode electrode in batteries on a large scale. However, the electrode of Zn reveals limited use in secondary alkaline batteries [12]. This problem can be ascribed to the shorting cycle life of Zn during the charging-discharging process [13]. This problem can be ascribed to the formation of dendrites and the change of electrode shape during the recharge process [14]. This indicates that the formation of $Zn(OH)_2$ on the surface (discharge product) in the concentrated alkaline electrolyte leads to shape change and dendrite formation [15]. Therefore, the change of shape can be ascribed to the continuous decrease of the active surface area of the zinc electrode during the repeated cycling of the battery. Hence, Zn alloyed with both Ni and In has the ability to retard the formation of dendrite significantly. Consequently, the Zn anode becomes more reversible [16]. Jo et al. [17] revealed that adding Bi to Zn has a great influence on inhibiting corrosion and hence promises to be utilized as an anode in Zn-air batteries.

Zn-air batteries have many applications, such as in the military, hearing aids, and railway signals [18,19]. Although Zn-air batteries have great potential, some problems observed during the anodic process, such as passivation, should be solved [1,7]. As a result of the anodic dissolution process of zinc in an alkaline solution, $[Zn(OH)_4]^{2-}$ is formed near the surface of the electrode. Hence, insoluble $Zn(OH)_2$ and ZnO are adsorbed on the surface of the zinc electrode when the solution becomes saturated with $[Zn(OH)_4]^{2-}$ [20]. Thus, the zinc electrode surface becomes passive. Stamm et al. [21] stated that passivation was formed on the surface of zinc as a result of the generation of ZnO and $Zn(OH)_2$. Thus, poor conductivity occurs, leading to a sharp decrease in the lifetime of alkaline-air batteries. Consequently, suppressing both passive films formed throughout the process of discharging and the hydrogen evolution on the Zn electrode surface leads to improvement in alkaline Zn battery performance. In our previous works [22], minor In alloyed with Zn has been studied on both cathodic and anodic processes in the active region, and other publications [23,24] on the anodic dissolution at different positive potentials have investigated. The results show that small alloying of In with Zn has a good effect on charge reliability, capacitance, and hydrogen evolution reaction attenuation. These publications (under anodic studies) show that the indium metal alloyed with zinc metal significantly improves impedance behavior, lifetime, charge efficiency, and capacitance in the passive region.

According to a survey of relevant literature, there is no published research on the anodic behavior of the alloy of Zn-Sb produced in

†To whom correspondence should be addressed.
E-mail: dr_mahmoudelrouby@hotmail.com, elsayed777@yahoo.com

our laboratory through the fusing process. Our previous work [25] was devoted to the characterization of the prepared alloy with two different Sb contents (as a novel alloy), and the electrochemical behavior was studied in the range of Tafel plots only (active region). The 1% Sb as an alloying element with Zn results in a high corrosion protection efficiency (98.5%). This suggests that increasing the amount of minor Sb in alkaline batteries improves hydrogen evolution suppression, charge efficiency, durability, and capacitance. After the development of the passive film, the current study complements the prior work of part I, which used several electrochemical methods such as galvanostatic impedance spectra (EIS), and charge-discharge investigations. The present work is devoted to examining the effect of small content of Sb alloyed with Zn on its passivation and passivity breakdown in the basic electrolyte. The inclusion of Sb in the alloy is predicted to slow passivation and facilitate passivity breakdown at higher positive potentials. As a result of the increased conductivity on the alloy surface, alkaline Zn battery charge efficiency, longevity, and specific capacitance will enhance in the passivity zone.

EXPERIMENTAL

1. Materials

A stock electrolyte of 6 M KOH was obtained by dissolution of the evaluated weight from KOH (analytical grade) in doubly distilled water. Metals of zinc and antimony with high purity grade (99.99%) were obtained from Jonson Matthey Chemicals Ltd. The two metals were utilized in the preparation of zinc-antimony alloy with two Sb contents (0.5% Sb and 1% Sb by weight) by the fusion method [26-28]. The estimated amounts of the two mentioned metals were mixed and introduced into closed, evacuated silica tubes. Afterward, the tubes were fused in a muffle furnace (Gallenkam) at 750 °C for 24 hr. To obtain molten homogeneity, shaking every six hours of the tubes in the same used muffle furnace was done. Hence, as reported, this fusion was quenched in cooled water [29]. The prepared alloys were cut as rods, and each sample had a surface area of about 0.196 cm^2. Those electrodes were produced using the rods mentioned above of pure zinc and Zn-Sb alloys and were individually placed into a Teflon rod and sealed with epoxy glue. The exposed surface area of the fabricated electrodes in the solution was 0.196 cm^2. In a prior study, we used XRD and SEM to characterize the produced alloys and identify the phases generated on the alloy surface [25].

2. Electrochemical Examinations

Versastat 4 Potentiostat/Galvanostat was utilized in all electrochemical experiments under investigation. The volume capacity of the electrolytic cell, which was utilized in the electrochemical measurements, about 250 ml, and the cell is of a three-electrode system. The design of the cell was reported in the previous work [30]. The surface of each studied electrode was manually cleaned using consecutive emery paper grades (1,000-1,200 μm) before each investigation. Then, they were rinsed and washed with pure ethyl alcohol and double-distilled water, respectively, before being inserted into the electrolytic cell. A reference and counter electrodes of saturated calomel and Pt sheet, respectively, were used in all electrochemical measurements. Each investigated specimen surface was fixed at −2.0 V for five minutes in the investigated alkaline electrolyte to eliminate any oxides generated on the electrode surface. After that, the polarization of the electrode was disconnected by shaking the cell to remove the hydrogen gas which was adsorbed on the surface of the electrode. Then, the electrochemical performance of each electrode was examined. The galvanostatic technique should be utilized to get more precise data about the anodic dissolution and passivation of the examined electrodes in the studied electrolyte. The effect of small Sb alloyed with Zn was studied on the potential/time transients at various current densities (50 to 80 $mA \cdot cm^{-2}$) and 25 °C. Before starting EIS experiments, a passive layer was formed on each specimen surface at three different positive potentials (+0.5, +0.8, and +2.0 V). The amplitude of AC potential was 10 mV, and the frequency range started from 10 kHz to 1 Hz. Before the measurements of the charge-discharge process, a passivated layer was produced at an applied certain value of potential equal to +0.8 V in the studied electrolyte for 20 min by the potentiostatic test. Then, the discharge process using galvanostatic measurements was examined at various densities of current (−40, −50, −60, −70, and −90 $mA \cdot cm^{-2}$).

RESULTS AND DISCUSSION

1. Anodic Behavior Using Galvanostatic Measurements

The galvanostatic technique was used to get more knowledge about the effect of small antimony alloyed with zinc on its passivation and passivity breakdown in the concentrated alkaline solution (6 M KOH). The anodic polarization of potential-time transient of Zn specimen and Zn-Sb alloy (0.5 and 1%Sb) electrodes at various densities of current (50 up to 80 mA cm^{-2}) is exhibited in Fig. 1. Those curves exhibit that the potential of anodic polarization in the region AB can be nearly stable (the behavior of active region). Thus, beginning from point B up to C (BC region), the potential starts to rapidly rise to higher potential values, with mainly linear changing. This trend can be ascribed to a decrease of hydrogen overpotential and, in addition to the electrical double layer between the surface of metal and electrolyte interface, is charged [31]. Moreover, the density of the current value, which is used in the polarization in addition to the concentration of the solution, plays an important role in in this process [32]. Thus, when this behavior reaches the maximum value, the change in the potential of the zinc electrode becomes slower with time. This reveals that the surface of the electrode is not completely covered by the oxide film. Consequently, the dissolution of Zn to Zn^{2+} ions continues through the porous layer [33].

Therefore, the AB region means that the rate of Zn dissolution on the surface is approximately equivalent to the rate of formation for the oxide layer. Consequently, when the formation of insoluble oxide or hydroxide of Zn on its surface is predominant (BC region), passivation process occurs. This means that the OH^- ion diffusion to the electrode surface is retarded, preventing the formation of zincate ions. Thus, Zn metal is oxidized directly to ZnO. Accordingly, the potential region of BC can be attributed to the following reactions [24]:

$$Zn \rightarrow Zn^{2+} + 2e \quad (1)$$

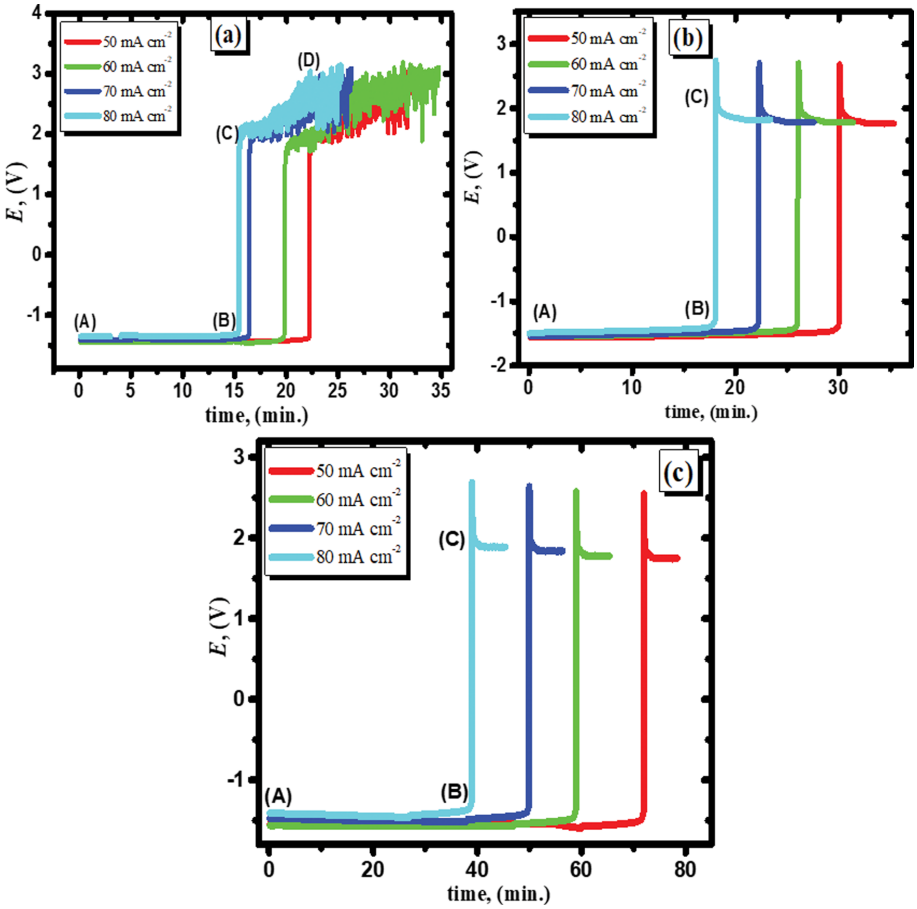

Fig. 1. Anodic polarization of potential-time curves of Zn (a) and its alloys I (b), and II (c) in the basic solution at various densities of current and at 25 °C.

$$Zn^{2+}+2OH^{-}\rightarrow Zn(OH)_2 \quad (2)$$

$$Zn(OH)_2\rightarrow ZnO+H_2O \quad (3)$$

Therefore, the dissolution of the anodic oxide film produced on the zinc electrode surface is lower than its formation [34].

After that, the voltage at part C tends to arrive at the steady-state value of passivation. The passing current density in this region can thus be assigned to the insoluble corrosion products formed on the specimen surface of Zn [30]. But, the curves of Zn in the CD region exhibit a very high oscillation in the potential-time behavior. This trend can be ascribed to the competition between the process of dissolution of the passivated layer generated on the surface and its formation [24]. And this can be attributed to the concentrated KOH solution's high dissolving power. On the other hand, all passive regions (at CD) at various imposed current densities seem to be similar. This indicates that the variation in the current density does not influence the process of passive film formation in this region. Generally, the nature and thickness of the passivation layer precipitated on the surface of the specimen are unaffected by variations in the imposed current density. This is demonstrated by the fact that the rate of passive layer growth on the specimen surface of Zn increases due to increasing current density. Consequently, the variation rate in potential increases rapidly with the increase of the applied current, up to reaching the potential to a certain steady-state value. Accordingly, the passivation time value ($t_{pass.}$) decreases as a result of increasing the imposed density of current. However, the steady state of potential is still nearly without change.

The data also in Fig. 1 (curves (b) and (c)) exhibited the potential-time behavior of the two investigated alloys (0.5 and 1% Sb) under the same conditions for the Zn electrode. Generally, there is no significant change in the general trend of the mentioned curves. But, it is worth seeing that a drop in the passivation potential is observed at arrest C of the two examined alloy samples. This represents that some collapse of the passivation film on the alloy occurred [35]. Due to Sb alloying, the assigned trend could be ascribed to the dissolution of the oxide film formed on the specimen. Gileket et al. [36] stated that the formation of Sb_2O_3 or Sb_2O_5 on the surface is easily dissolved in NaOH solution. This trend is consistent with the data of both potentiodynamic and potentiostatic measurements (part I). It is interesting that the great vibration in the potential, which is noticed in the curves of pure Zn specimen (CD region), is not observed in alloy specimens due to Sb alloying with Zn metal. This observation could be discussed on the premise that the breakdown of the passivated film at C arrest leads to a continuous dissolution process on the alloy surface more than its formation [24]. The mentioned graphs of the zinc specimen and alloyed zinc with minor antimony content in the investigated basic elec-

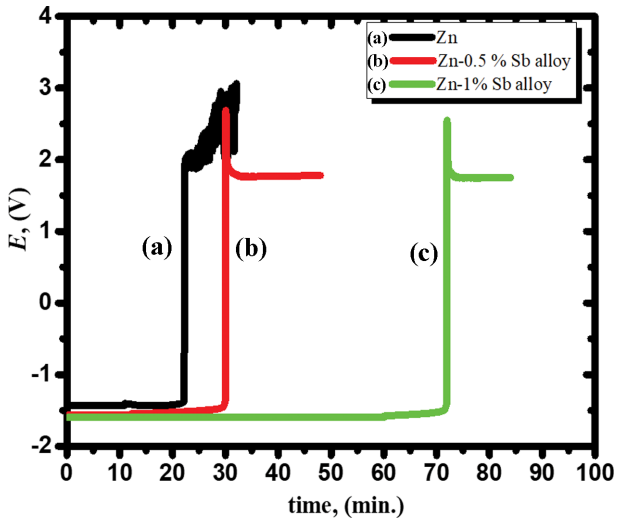

Fig. 2. Relation between anodic polarization potential and time of Zn specimen (a), and its alloys I (b) and II (c) in the concentrated basic electrolyte at 50 mA cm^{-2} and 25 °C.

trolyte at 50 mA cm^{-2} and 25 °C are compared (Fig. 2). It is interesting that the passivation time ($t_{pass.}$) is prolonged with the increase of trace alloyed Sb with Zn. This trend is illustrated on the basis that minor Sb alloying with Zn metal promotes the dissociation of Zn and passivity breakdown.

By comparing the data of the studied alloy with that of the previous work [24] of Zn-In alloy in the same investigated solution, the opposite behavior was observed. This behavior shows that In alloying with Zn decreases the passivation time ($t_{pass.}$), indicating the poor electron conductance of the passive film [37]. This trend proves the diminishing of $t_{pass.}$ (as a result of adding indium to zinc) in comparison to that of zinc, which can be attributed to the formation of more stable In_2O_3 in addition to ZnO on the surface. This confirms that Zn-In alloy tends to be more passivated than Zn-Sb alloy in the same investigated electrolyte solution. Accordingly, the reactions of the electrochemical dissolution process on the alloy surface can be indicated as follows:

$$Zn+2OH^- \rightarrow Zn(OH)_2 \quad (2)$$

$$Zn(OH)_2+2OH^- \rightarrow [Zn(OH)_4]^{2-} \quad (4)$$

At the same moment, Sb also dissolves as $[Sb(OH)_4]^-$ or $[Sb(OH)_6]^{3-}$ as shown in the following reactions:

$$Sb+OH^- \rightarrow (SbOH)_{ads}+e \quad (5)$$

$$(SbOH)_{ads}+OH^- \rightarrow (SbO)_{ads.}+H_2O+e \quad (6)$$

$$(SbO)_{ads.}+OH^- \rightarrow HSbO_2+e \quad (7)$$

These reactions are followed by chemical dissolution to give $[Sb(OH)_4]^-$ or $[Sb(OH)_6]^{3-}$ complex ions:

$$HSbO_2+OH^-+H_2O \rightarrow [Sb(OH)_4]^- \quad (8)$$

and/or

$$HSbO_2+3OH^-+H_2O \rightarrow [Sb(OH)_6]^{3-} \quad (9)$$

Therefore, in the active region Sb is dissolved as $[Sb(OH)_4]^-$ or $[Sb(OH)_6]^{3-}$. But, in the region of BC, the potential of anodic polarization begins to increase very quickly. This observation can be ascribed to the precipitation of ZnO in addition to Sb oxides on the surface. Consequently, these oxides are significantly retarding the dissolution process.

The generation mechanism of the oxide film on the surface of the alloy can be explained according to the production of saturated solutions from $[Zn(OH)_4]^{2-}$ and $[Sb(OH)_4]^-$ around the electrode surface. Therefore, the mechanism of dissolution-precipitation can be applied to the passive film formed according to the equilibrium reactions as follows:

$$[Zn(OH)_4]^{2-} \leftrightarrow Zn(OH)_2+2OH^- \quad (10)$$

$$[Sb(OH)_4]^- \leftrightarrow Sb(OH)_3+OH^- \quad (11)$$

Then, dehydration of these hydroxides takes place; consequently, more stable oxides of both Zn and Sb are formed [38]:

$$Zn(OH)_2 \rightarrow ZnO+H_2O \quad (3)$$

and/or

$$2\,Sb(OH)_3 \rightarrow Sb_2O_3+3H_2O \quad (12)$$

A similar mechanism of dissolution-precipitation of Sb-Sn alloy in KOH solution was reported by El-Sayed et al. [29], who showed that a layer from Sb_2O_3, in addition to SnO, was formed on the alloy surface. Therefore, the potential rises significantly with time in the anodic direction, and the active dissolution on the surface is suppressed.

The data in Fig. 3 reveal the relation between the arrest ($E_{ar.}$) of the initial potential and the current density of the Zn specimen and its studied alloy specimens as electrodes in the mentioned basic electrolyte. The curves in Fig. 3 show that the arrest $E_{ar.}$ of the initial potential moves to more positive values with the increase of the applied density of current (I), as shown in the following equation [20,39].

$$E_{ar.}=E_{i=0}+ZI \quad (13)$$

where the measured potential is $E_{ar.}$ of each electrode sample, while the potential at a current density equal to zero is $E_{i=0}$ and the constant is Z.

It is interesting to observe that a straight line (curves in Fig. 3) of the mentioned relation is obtained. A high correlation coefficient (R^2>0.997) was obtained from the statistical analysis data of both Zn and alloy electrodes. Note that the value of $E_{i=0}$ can be evaluated from the intersection of the mentioned lines (Fig. 3) with the axis of potential, and the estimated values equal to −1.40, −1.480, and −1.520 V vs. SCE of the Zn, alloy specimens I and II, respectively. Therefore, the arrest of the estimated potentials was compared with the experimental values of ZnO and found to be nearly the same [40]. However, the more negative shifting in the potential with increasing Sb quantity in the alloy indicates that the surface is activated. Finally, one can conclude that the mentioned potential range is required for ZnO formation.

On the other hand, the formation of Sb_2O_3 occurs after the pre-

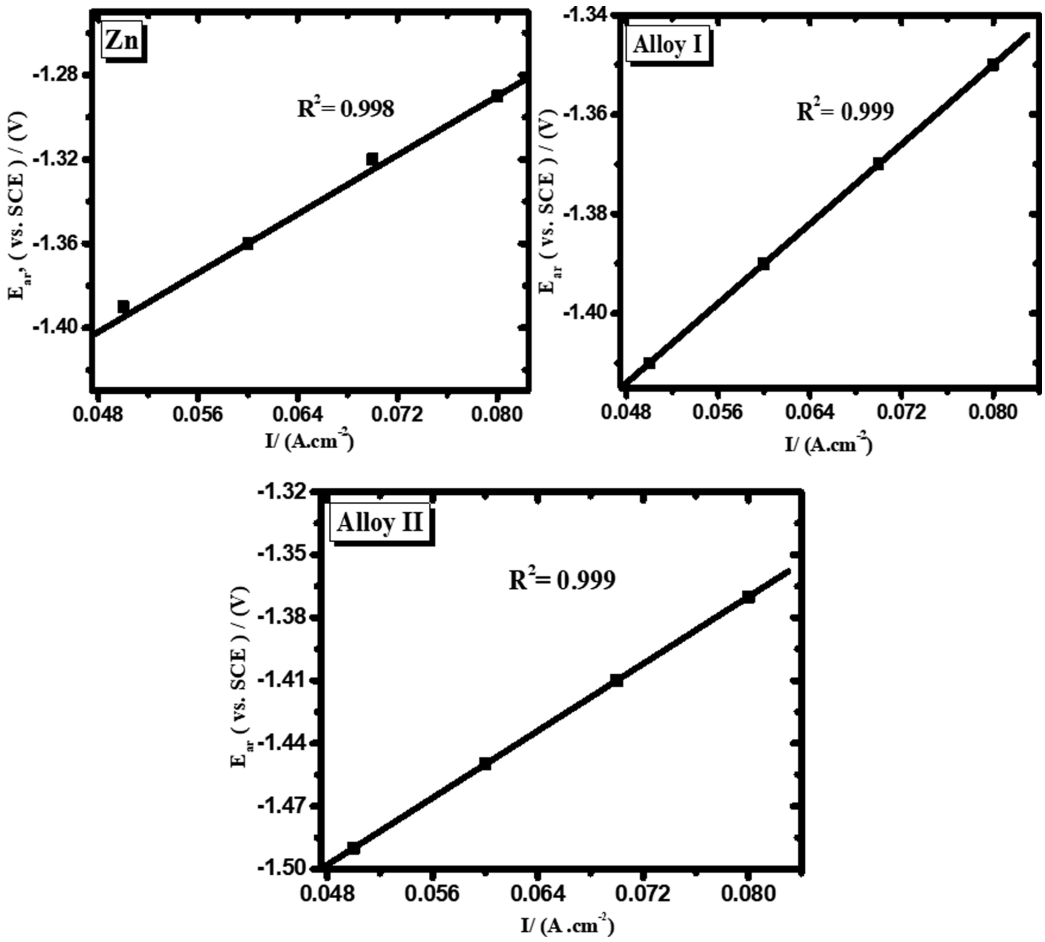

Fig. 3. Variation of the initial potential of arrest, $E_{ar.}$, with the applied current density of Zn specimen (a) and its alloys I (b) and II (c), in concentrated alkaline electrolyte and at 25 °C.

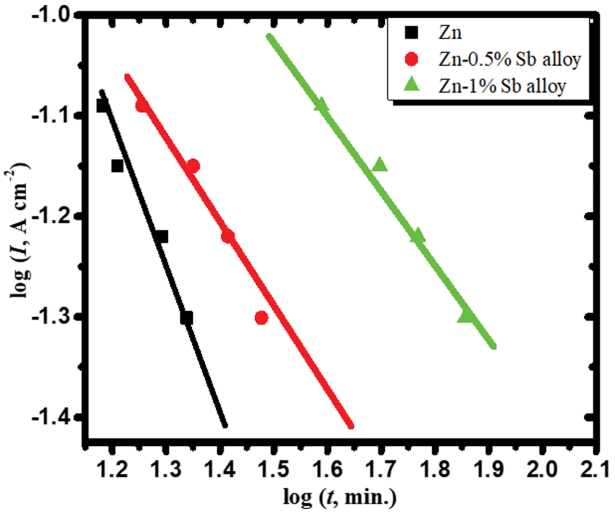

Fig. 4. Effect of imposed current density on passivation time (t) of Zn specimen (a), Zn-0.5% Sb (b), and Zn-1% Sb specimens (c) in concentrated basic media and at 25 °C.

cipitation of zinc oxide on the mentioned alloy surface.

Fig. 4 exhibits the influence of applied current density variation on the duration time of the passivated layer generated on the surface. It is fascinating to observe that the required time for the anodic process arrest is gradually decreased as the imposed current increases. This pattern could be described by OH^- ions diffusion from the solution bulk into the surface of the electrode, which decreases the distance of the induction period time [41]. Therefore, the diffusion of OH^- ions into the surface increases gradually with increasing the applied current. The potential under the anodic process begins to grow linearly with time after reaching passivation time. At this step, a sufficient passivated film has been produced on the surface of the electrode. Consequently, the formation rate of the passivity layer will be greater than that of its dissolution [31]. Hany et al. [41] revealed that ionic conduction causes continuous oxide growth on the surface. The value of $(dE/dt)_i$ is the rise in the steady-state potential at the fixed current density. This value is ascribed to the formation of an amorphous film. Consequently, a barrier to the dissolving process occurs under anodic polarization using the galvanostatic technique. The following equation can be considered the relation between $(dE/dt)_i$ values and the applied densities of current [42].

$$(dEldt)_i = a(i)^b \quad (14)$$

$$\log(dEldt)_i = \log a + b \log i \quad (15)$$

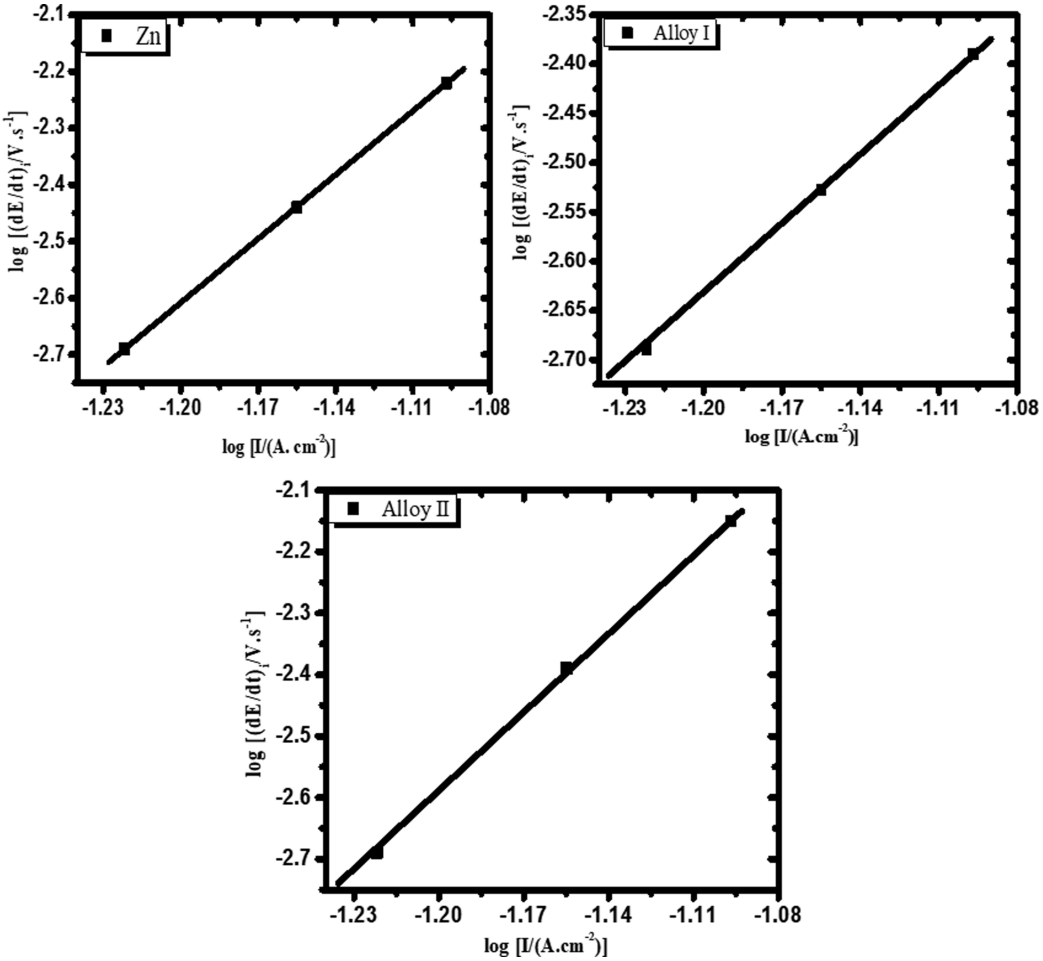

Fig. 5. A logarithmic relationship between the rate of oxide film generation $(dE/dt)_i$ and the imposed current density for Zn specimen (a), alloy I, and II (c) in the concentrated basic solution and at 25 °C.

where the constant values are a and b, which are characterized by the metal/electrolyte interface [31]. According to the above-mentioned equation (Eq. (15)), the variation of log $(dE/dt)_I$ with log i exhibits a linear relationship (Fig. 5). However, the constant b value (the slope of the straight line in Fig. 5) was found to be higher than 1.0. This indicates that the part from the imposed density of current was consumed in the dissolution of the passive film [24]. Wittman et al. [20] stated that the slope magnitude (b constant) should not exceed unity, which means that all applied current densities are not used completely in oxide film formation. Accordingly, the present data in Fig. 5 show that the efficiency of the ionic process is less than 100%.

The curves in Fig. 6 show the impact of the Sb percentage on the polarization arrest of duration time at different imposed current values. It can be noted that the duration time (t) increases gradually as a result of increasing the Sb percentage in the alloy. This implies that the rate of oxide generation on the surface of the alloy specimen decreases with increasing small Sb alloying. In other words, Zn-Sb alloy has the ability to become less passive with the addition of Sb to Zn compared with that of the Zn specimen. Along with a gradual increase in the $t_{pass.}$ with increasing small Sb alloyed with Zn can be ascribed to that a part of Sb ions was introduced in the ZnO lattice [43].

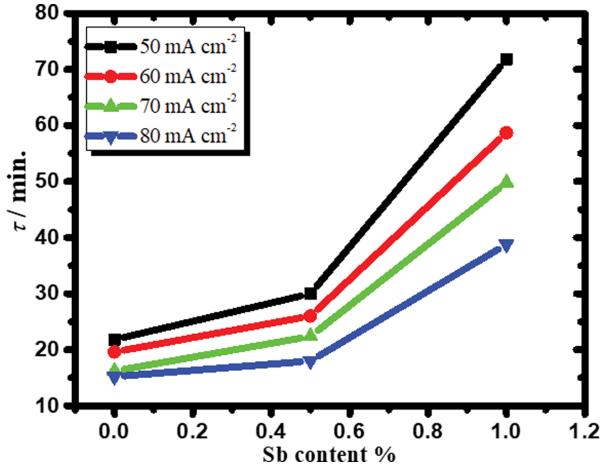

Fig. 6. Variation of duration time (t) of anodic polarization in the concentrated basic solution at various current densities as a function of Sb percentage in the alloy.

Therefore, the zinc ion diffusion rate from the interface between metal and film into the interface between film and solution is enhanced, and for this reason, vacancies of cations are formed. Accord-

ingly, some parts from the passive layer are broken, which proves that the surface of the alloy is refreshed in the passivity area. This means that the layer produced on the zinc electrode (including ZnO and $Zn(OH)_2$) is thicker and more protective than that of ZnO with Sb oxides together on the alloy surface.

2. Electrochemical Measurements on the Passivity Layer Produced on the Electrode Using the EIS Technique

Prior to the impedance spectra (EIS) measurements, a fixed potential was imposed on the investigated electrodes for 20 minutes in the alkaline solution at various potentials of the passive region

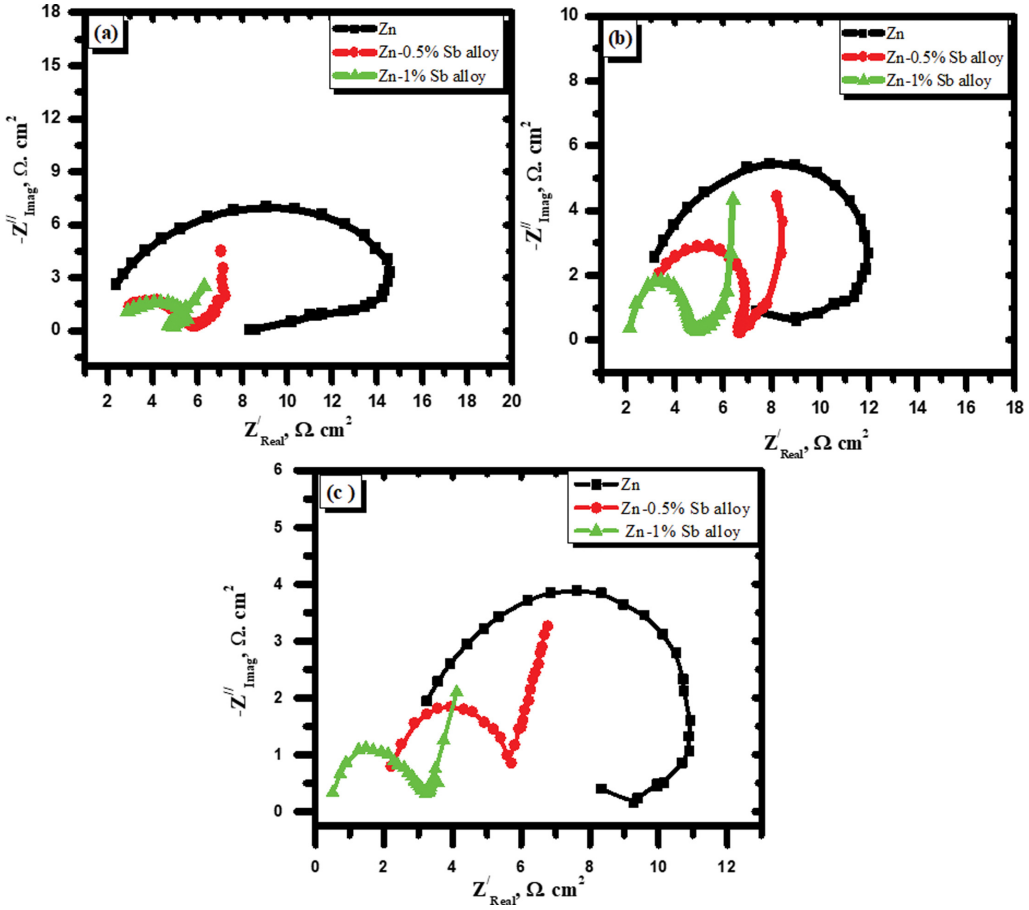

Fig. 7. Comparison between the experimental data of Nyquist plots of the Zn specimen and its alloys I and II in a concentrated alkaline solution of the passive film formed at various positive values of the potential of +0.5 V (a), +0.8 V (b), and +2.0 V (c), at 25 °C.

Table 1. Impedance characteristics for corrosion of Zn and its alloys tested at various potentials, the frequencies ranging from 10 kHz to 1 Hz in 6 M KOH at 25 °C

Parameters	Z_w (Ω^{-1} $S^{1/2}cm^{-2}$)	C_{dl} (F)	$R_p\Omega$	$R_s\Omega$
		At applied potential +0.5 V		
Zn	-	1.17×10^{-6}	13.5	2.2
Zn-0.5% Sb alloy	0.190	2.5×10^{-6}	6.3	2.5
Zn-1% Sb alloy	0.147	3.1×10^{-6}	5.2	2.5
		At applied potential +0.8 V		
Zn	-	1.47×10^{-6}	10.8	2.5
Zn-0.5% Sb alloy	0.176	2.6×10^{-6}	6.1	2.5
Zn-1% Sb alloy	0.123	3.4×10^{-6}	4.7	1.7
		At applied potential +2.0 V		
Zn	-	1.56×10^{-6}	10.2	2.5
Zn-0.5% Sb alloy	0.15	3.2×10^{-6}	4.9	2.0
Zn-1% Sb alloy	0.110	5.0×10^{-6}	3.2	0.4

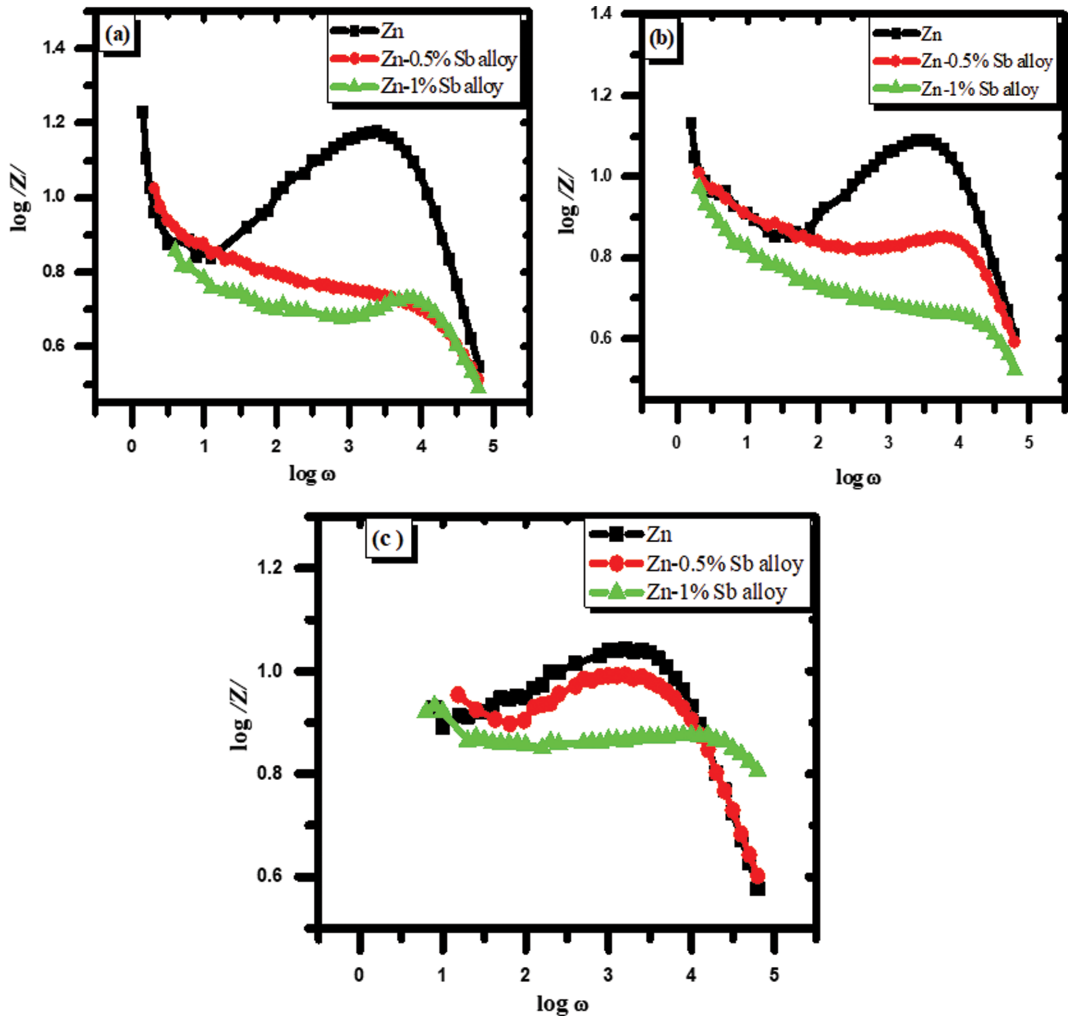

Fig. 8. Comparison between experimental data of Bode plots Zn specimen and its alloys I and II of the passive film formed at various positive potentials of +0.5 V (a), +0.8 V (b), and +2.0 V (c), at 25 °C.

(+0.5, +0.8, and +2.0 V vs. SCE) and 25 °C using potentiostatic technique. The electrolytic cell was then opened in the same investigated solution for 30 minutes (without polarization) to establish a constant potential (steady-state) before initiating the EIS measurements. The experimental measurements of EIS of the studied electrodes in the mentioned electrolyte on the passive film formed at different potentials (+0.5, +0.8, +2.0 V vs. SCE) are displayed in Fig. 7 as Nyquist plots. Also, the plots of Bode curves are shown in Fig. 8. The parameters of EIS experiments such as $R_{ct.}$ and C_{dl} were estimated using the spectrum of impedance from Nyquist and Bode plots, respectively, and cited in Table 1. However, the value of the Warburg impedance (Z_w) was calculated utilizing the equations as follows [44]:

$$Z' = \sigma\frac{1}{\sqrt{\omega}} - i\frac{1}{\sqrt{\omega}} \tag{16}$$

$$|Z| = \sqrt{\frac{2\sigma}{\omega}} \tag{17}$$

The following slope was used in the evaluation of σ (Warburg coefficient). Accordingly, Warburg impedance was estimated from Eq. (18):

$$Z_w = \frac{1}{\sigma\sqrt{2}} \tag{18}$$

The data in Fig. 7(a), (b), (c) exhibit the experimental EIS as Nyquist plots for Zn and Zn-Sb alloy. EIS data reveal that the semicircle plots are not ideal, which may be due to the roughness on the surface, leading to the dispersion process. Consequently, the double layer of the studied electrodes deviates from the pure capacitance [45]. It is interesting that, at higher frequencies (HF), nearly semicircle plots are observed, which can be attributed to charge transfer resistance ($R_{ct.}$), after that a Warburg tail (Z_w) appears at the low frequencies (LF) for Sb alloyed with Zn at all examined potentials. However, the Warburg line is not observable in the passive zone at lower frequencies when using a pure Zn electrode. This indicates that the passivation process occurs as a consequence of $Zn(OH)_2$ and ZnO formation; consequently, its dissolution process is retarded [21]. Therefore, the passive film generated on the zinc specimen's surface acts as a barrier of OH^- ions diffusion. For

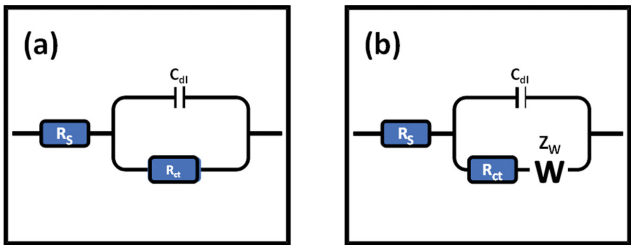

Fig. 9. Equivalent circuit models designed to evaluate the obtained practical data at various positive values of the potential of Zn specimen (a) and its alloys (b).

this reason, the interaction between the bulk of the surface and OH^- ions is suppressed. The appearance of a Warburg tail occurs as a consequence addition of Sb to Zn. This trend can be attributed to the diffusion of dissolving ions through pores that are formed on the alloy surface to the main bulk of the electrolyte [46]. This implies that the passivated film generated on the surface of the alloy is electron-conducting [47], which means that the conductivity can be assigned to the presence of Sb as ions in the passivated film [48]. Due to dissolving Sb oxides present on the surface and diffusing to the bulk of the solution, pores in the passive film are generated. Therefore, new reactions start on the surface of alloy specimens as a result of easily reaching OH^- ions to the electrode surface. Also, the addition of Sb as an alloying element can improve the capacity and efficiency of the Zn anode in alkaline batteries [49]. The impedance results were simulated using the equivalent circuit, as shown in Fig. 9(a) and (b) [50]. $R_{ct.}$ and C_{dl} values are simulated using the equivalent circuit for Zn electrode only at different potentials in the passive region (Fig. 9(a)). But, Fig. 9(b) shows the equivalent circuit which is used in analyzing the results of impedance for Zn-Sb alloy (0.5% Sb and 1% Sb). This equivalent circuit includes the solution resistance (R_s), $R_{ct.}$, and $C_{dl.}$ in addition to Z_w (Warburg impedance). The calculated impedance parameters of both zinc metal and its investigated alloy specimens (I and II) are cited in Table 1. The data in this table reveal that the $R_{ct.}$ and Z_w decrease, while the value of $C_{dl.}$ rises gradually as Sb amount increases at all examined values of potential in the passive area. This phenomenon may be explained by the fact that adding tiny quantities of Sb to Zn increases the porosity of the passivated film that forms on the alloy [33]. Therefore, the passive layer becomes less protective, and OH^- ions easily reach the surface. Accordingly, the reaction kinetics is controlled by OH^- ions diffusion, and the products of the oxidation reaction through the pores in the passive layer go away from the surface [51]. Then, new reactions start on the surface of the alloy specimen, which is due to easily reaching OH^- ions. Consequently, the oxide layer on the alloy becomes easily attacked by the OH^- ions diffusion [44], and the breakdown of some parts from the passive film occurs.

The results also in Table 1 exhibit that the anodic passive film formed at various applied potentials shows the value of $R_{ct.}$ is less, while the value of $C_{dl.}$ is greater at high positive voltage than that of a low positive one. This indicates that the oxide layer formed at a more positive volt is less protective due to the high dissolution of this film. On the other hand, the values of Z_w are estimated only for the two investigated alloys at the different mentioned potentials. The data of Z_w values reveal that the value also decreases with the shifting potential to a more positive direction, which is used for oxide film formation. It can be noted that the Z_w of the Zn-1%Sb specimen is lower in comparison to that of Zn-0.5%Sb one at all investigated potentials. This trend of the low Z_w values with increasing Sb amount in the alloy specimen can be ascribed to the fast process of diffusion for the dissociated species [49]. Thus, when the $R_{ct.}$ value decreases, the electrochemical polarization decreases, but the surface activity increases, resulting in high electronic conductivity. The data obtained from impedance measurements are confirmed by the results obtained from the galvanostatic measurements.

3. Measurements of Charge-discharge Performance Using the Galvanostatic Technique

To examine the effect of a small Sb amount alloyed with zinc metal on its behavior as an anode electrode in the cells of an alkaline battery on the passive layer, which was formed before the experiments, galvanostatic charging-discharging measurements were studied. Before these measurements, the oxide layer was produced on each surface of the sample in the mentioned alkaline electrolyte at +0.8 V vs. SCE for 20 min using the potentiostatic technique. The data obtained from the galvanostatic charge-discharge of the studied electrodes (Zn metal and its alloys) in the examined solution are displayed in Fig. 10. The current density used in this investigation was ±0.09 $A{\cdot}cm^{-2}$. Note that the charge-discharge cycling of the minimal Sb alloyed with Zn is greater than that of the Zn anode. The behavior shows that adding Sb to Zn improves life duration, ion mobility, and conductivity [52]. According to the obtained measurements, the difference in potential (ΔV) of Zn and alloys I and II is 0.38, 2.47, and 1.1 V, respectively. This implies that ΔV values of investigated alloy specimens were greater than that of the Zn electrode at a fixed period (t). It is fascinating to observe that alloy I revealed the highest value compared with that of both Zn and alloy II. This means that the passivated film produced on the alloy surface gets increasingly electron conducting. Therefore, 0.5% Sb alloyed with Zn has the ability to increase the

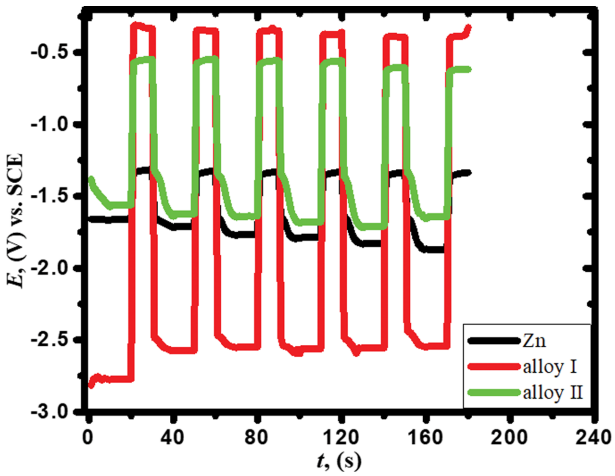

Fig. 10. Galvanostatic charge-discharge curves of zinc and its alloy I and II electrodes in the concentrated basic electrolyte at ±0.09 $A{\cdot}cm^{-2}$ as applied current density and at 25 °C.

efficiency of energy to a larger extent than that of Zn and alloy II. Accordingly, minor Sb alloyed with Zn has a positive influence on increasing the capacity of the zinc electrode, and the optimal percentage of Sb in the alloy is 0.5%.

The obtained results could be illustrated based on the reaction of hydrogen liberation on the surface of the alloy being significantly suppressed, in addition to Zn ions which are near from the alloy surface and are easily reduced [25]. The lower potential value observed of the zinc electrode compared to that of the Zn-Sb alloy can be ascribed to the production of ZnO and $Zn(OH)_2$ during the discharge process. Consequently, the generation of a thick layer on the zinc specimen surface occurs, leading to a barrier of diffusion of OH^- ions [21]. Thus, adding a small quantity of Sb to zinc metal inhibits the generation of $Zn(OH)_2$ and reduces the amount of ZnO generated on the alloy surface by breaking down the passive layer. This observation can be interpreted on the basis that adding small Sb to zinc metal can enhance the conductivity of the passivity film. Consequently, the discharge performance and charging efficiency are improved [53].

The results obtained from galvanostatic and EIS measurements confirm this illustration that the impedance of the charge transfer process is retarded with the addition of Sb. The stability of the practical discharge of the studied electrodes has been done for 100 cycles (Fig. 11). The data clearly show that the discharge capacity seems to be unchanged (stable) with a cycling process up to 100 cycles at $-0.09\ A{\cdot}cm^{-2}$ as the applied current of pure Zn electrode and its investigated alloys.

The obtained data reveal that the examined electrodes have high stability. However, the discharge capacity of Zn-0.5% Sb is higher than that of pure Zn and Zn-1%Sb alloy electrodes. This implies that the little addition of 0.5%Sb to Zn has a significant impact on enhancing the electrical conductivity. Consequently, the charge transfer on the alloy surface is also improved, leading to the improvement of the charge/discharge process [45]. The specific capacitance of the investigated anodes in the examined electrolyte at different current densities was evaluated (Fig. 12).

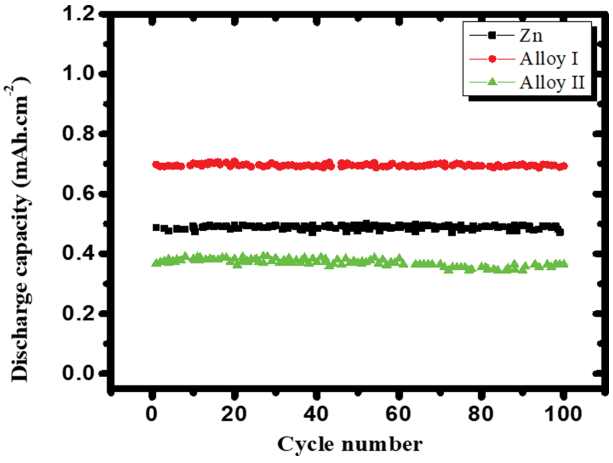

Fig. 11. The relation between discharge capacity and cycle number of Zn and its alloys I and II electrodes in the concentrated basic electrolyte at the generation of the passive layer at +0.8 V and -0.09 A·cm^{-2} as current density.

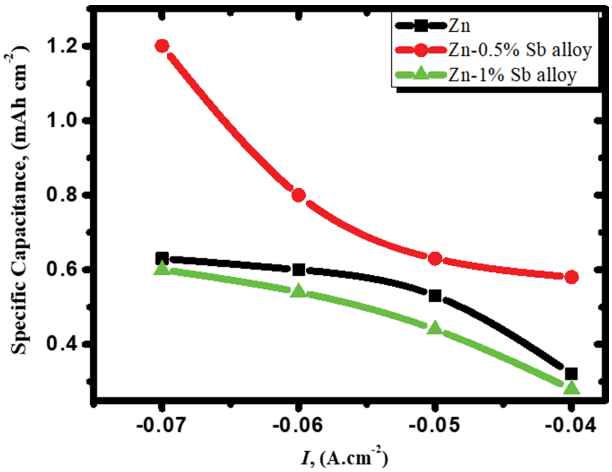

Fig. 12. Variation of specific capacitance for Zn specimen and its alloys I and II with the imposed current density in the concentrated basic electrolyte of the passive layer formed at +0.8 V and 25 °C.

It can be noted that the specific capacitance was raised with a small addition of Sb (0.5%) to Zn and also with increasing current density [24]. However, this capacitance slightly decreased at 1% Sb alloyed with Zn compared to the pristine Zn. This tendency may be explained by the fact that a larger Sb (1%) proportion in the alloy causes a passivity breakdown on the alloy surface. Consequently, higher dissolution occurs compared with that of lower content (0.5%Sb). This phenomenon may be traced back to the surface exposed to KOH solution more directly.

More specifically, a 1% Sb alloyed with Zn results in a reduction in discharge-specific capacitance, which may be attributed to traces from Sb being oxidized to Sb oxides, lowering the mass ratio of Zn [47]. In addition, 1%Sb alloying leads to the film's structure on the surface becoming disordered, leading to less electrochemical activity. Accordingly, the mentioned alloy (particularly at 0.5% Sb) exhibited a lower corrosion process, longer discharge time, and greater capacitance than the Zn electrode.

CONCLUSIONS

The influence of small Sb alloyed with Zn on its passivity and passive breakdown in the basic solution of 6 M KOH (which is used in alkaline batteries) was investigated utilizing different methods, such as galvanostatic, EIS, and charge-discharge. The obtained results of the galvanostatic measurements reveal anodic polarization curves of the relationship between the potential and time of the zinc electrode and Zn-Sb specimen (including two percent contents by weight of Sb) in the electrolyte at different values of current. Alloyed Zn with minor Sb element shows a prolonged time in t_{pass}. This implies that a small quantity added of Sb to Zn promotes its dissolution in the active region, in addition to the passivation film being destroyed at more positive potentials. This reveals that the dissolution process of the alloy was enhanced compared with that of the Zn electrode. This demonstrates that the passive layer on the surface of the alloy is less compact and more porous. Also, adding minor Sb to Zn influences to suppress the great oscil-

lation in potential, which is noticed in the Zn electrode at high positive potential. This observation can be assigned to the continuous dissolution process on the alloy surface more than the passive layer formed on its surface. The data obtained from EIS on the passive layer formed on each surface at various potentials show that the magnitudes of R_{ct} and Z_w diminish, while the magnitude of C_{dl} enhances with increasing the Sb amount in the alloy at all studied potentials. However, the magnitudes of R_{ct} and Z_w decrease, while C_{dl} magnitude increases of the passive film generated at the more positive potential in comparison to these at the less positive one. The data of the charge-discharge process reveal that the difference in potential (ΔV) of the studied electrodes is 0.38, 2.47, and 1.1 volt of zinc and alloy specimens I and II, respectively. This behavior shows that the energy density and charge efficiency are significantly enhanced by including a small quantity of Sb to Zn, and the highest values are obtained of alloy I. Along with this, the specific capacitance becomes more promoted with the presence of 0.5% Sb in the alloy specimen. Finally, small Sb alloyed with Zn has a favorable effect on improving the capacity of the Zn electrode, with 0.5 percent Sb in the alloy being the recommended proportion.

CONFLICT OF INTEREST

The authors declared that they have no conflict of interest

AVAILABILITY OF DATA AND MATERIALS

All data generated or analysed during this study are included in this article.

REFERENCES

1. L. Yanguang and D. Hongjie, *Chem. Soc. Rev.*, **43**, 5257 (2014).
2. J. S. Lee, S. T. Kim, R. Cao, N. S. Choi, M. Liu, K. T. Lee and J. Cho, *Adv. Energy Mater.*, **1**, 34 (2011).
3. H. Ma and B. Wang, *RSC Adv.*, **4**, 46084 (2014).
4. M. Prabu, P. Ramakrishnan and S. Shahmugam, *Electrochem. Commun.*, **41**, 59 (2014).
5. G. L. Tian, M. Q. Zhao, D. Yu, X. Y. Kong, J. Q. Huang, Q. Zhang and F. Wei, *Small*, **11**, 2251 (2014).
6. Z. Shao, W. Zhang, D. An, G. Zhang and Y. Wang, *RSC Adv.*, **5**, 97508 (2015).
7. T. M. Bawazeer, A. M. El Defrawy and A. A. El-Shafei, *Colloids Surf. A*, **520**, 694 (2017).
8. A. Singh, K. R. Ansari and M. A. Quraishi, *Colloids Surf. A*, **607**, 125465 (2020).
9. J. Huang and Z. Yang, *RSC Adv.*, **5**, 33814 (2015).
10. J. Drillet, M. Adam, S. Barg, A. Herter, D. Koch, V. Schmidt and M. Wilhelm, *ECS Trans.*, **28**, 13 (2010).
11. P. Bonnick and J. Dahn, *J. Electrochem. Soc.*, **159**, A981 (2012).
12. W. Hong, Z. Jia and B. Wang, *J. Appl. Electrochem.*, **46**, 1085 (2016).
13. Y. Tian, Y. An, C. Liu, S. Xiong, J. Feng and Y. Qian, *Energy Storage. Mater.*, **41**, 343 (2021).
14. C. Zhang, J. M. Wang, L. Zhang, J. Q. Zhang and C. N. Cao, *J. Appl. Electrochem.*, **31**, 1049 (2001).
15. Y. Yu, Y. Zuo, Z. Zhang, L. Wu, C. Ning and C. Zuo, *Coatings*, **9**, 692 (2019).
16. C. W. Lee K., Sathiyanarayanan, S. W. Eom and M. S. Yun, *J. Power Sources*, **160**, 1436 (2006).
17. Y. N. Jo, K. Prasanna, S. H. Kang, P. R. IIango, H. S. Kim, W. S. Eom and C. W. Lee, *J. Ind. Eng. Chem.*, **53**, 247 (2017).
18. W. Gan, D. Zhou, L. Zhou, Z. Zhang and J. Zhao, *Electrochim. Acta*, **182**, 430 (2015).
19. M. Hilder, B. W. Jensen and N. Clark, *Electrochim. Acta*, **69**, 308 (2012).
20. R. M. Wittman, R. L. Sacci and T. A. Zawodzinski, *J. Power Sources*, **438**, 227034 (2019).
21. J. Stamm, A. Varzi, A. Latz and B. Horstmann, *J. Power Sources*, **360**, 136 (2017).
22. M. Elrouby, H. A. S. Shilkamy and A. Elsayed, *J. Alloys Compd.*, **854**, 157285 (2021).
23. A. Elsayed, H. A. S. Shilkamy and M. Elrouby, *J. Solid State Electrochem.*, **25**, 2161 (2021).
24. M. Elrouby, H. A. E. Shilkamy and A. E. R. Elsayed, *J. Solid State Electrochem.*, **25**, 2175 (2021).
25. A. ElSayed, H. A. S. Shilkamy and M. Elrouby, *Int. J. Hydrogen Energy*, **46**, 31239 (2021).
26. A. ElSayed, A. M. Sahker and H. M. Abd El Lateef, *Corrosion Sci.*, **52**, 72 (2010).
27. A. ElSayed, H. S. Mohran and H. M. Abd El Lateef, *Corrosion Sci.*, **52**, 1976 (2010).
28. H. S. Mohran, A. ElSayed and H. M. Abd El Lateef, *Solid State Electrochem.*, **13**, 1147 (2009).
29. A. ElSayed, A. M. Shaker and H. G. ElKareem, *Bull. Chem. Soc. Jpn.*, **76**, 1527 (2003).
30. H. M. Abd El Lateef, K. Shalabi, A. R. Sayed, S. M. Gomha and E. M. Bakir, *J. Ind. Eng. Chem.*, **105**, 238 (2022).
31. E. E. Abdel Aal, *Corrosion Sci.*, **45**, 641 (2003).
32. E. E. A. El-Aal, *Corrosion*, **55**, 582 (1999).
33. M. Bockelmann, L. Reining, U. Kunz and T. Turekab, *Electrochim. Acta*, **237**, 276 (2017).
34. A. Chiba, S. Tanaka, W. Inami, A. Sugita, K. Takada and Y. Kawata, *Opt. Mater.*, **35**, 1887 (2013).
35. E. E. Abd El-Aal, *Corrosion Sci.*, **45**, 759 (2003).
36. D. Gileket, A. Brzózka, K. E. Hnida and G. D. Sulka, *Electrochim. Acta*, **302**, 352 (2019).
37. A. ElSayed, H. S. Mohran and H. M. Abd El Lateef, *Corrosion Sci.*, **51**, 2675 (2009).
38. A. R. El-Sayed, H. S. Mohran and H. M. Abd El-Lateef, *J. Solid State Electrochem.*, **13**, 1279 (2009).
39. E. Bayol, A. A. Gurten, M. Dursun and K. Kayakirilman, *Acta Phys. Chim. Sin.*, **24**, 2236 (2008).
40. H. M. A. ElLateef, L. I. Aliyeva, V. M. Abbasov and T. I. Ismayilov, *Adv. Appl. Sci. Res.*, **3**, 1185 (2012).
41. H. M. A. EL-Lateef, A. R. ELSayed and H. S. Mohran, *J. Trans. Nonferrous Met. Soc. China*, **25**, 3152 (2015).
42. E. E. A. El-Aal, *Corrosion Sci.*, **50**, 41 (2008).
43. A. R. El-Sayed and H. M. El-Lateef, *Bull. Mater. Sci.*, **38**, 1 (2015).
44. A. O. Alnajjar, H. M. Abd El Lateef, M. M. Khalaf and I. M. A. Mohammed, *Constr. Build. Mater.*, **317**, 25918 (2022).
45. X. Zeng, Z. Yang, J. Long, L. Chen, H. Qin and M. Fan, *Ionics*, **25**, 1223 (2019).

46. A. R. El-Sayed, H. S. Mohran and H. M. A. El-Lateef, *J. Power Sources*, **196**, 6573 (2011).
47. L. Wang, Y. Liu, X. Chen and Z. Yang, *Electrochem. Soc.*, **164**, A3692 (2017).
48. J. He, Y. Wei, T. Zhai and H. Li, *Mater. Chem. Front.*, **2**, 437 (2018).
49. A. H. Abdalla, C. I. Oseghale, J. O. G. Posada and P. J. Hall, *IET Renew. Power Gener.*, **10**, 1529 (2016).
50. S. S. A. El-Rehim, H. H. Hassan and A. Mohammed, *Appl. Surf. Sci.*, **187**, 279 (2002).
51. M. Mouanga and P. Berçot, *Corrosion Sci.*, **52**, 3993 (2010).
52. P. Gu, M. Zheng, Q. Zhao, X. Xiao, H. Xue and H. Pang, *J. Mater. Chem. A*, **5**, 7651 (2017).
53. X. Chen, L. Wang, H. Qin and Z. Yang, *Ionics*, **25**, 1715 (2019).